

# Simple, fast and accurate evaluation of the action of the exponential of a rate matrix on a probability vector

Chris Sherlock<sup>1\*</sup>

<sup>1</sup>Department of Mathematics and Statistics, Lancaster University, UK

## Abstract

Given a time-homogeneous, finite-statespace Markov chain with a rate matrix, or infinitesimal generator of  $\mathbf{Q}$ , an initial distribution of  $\nu$  and a time interval of  $t$ , the distribution across states at time  $t$ ,  $\nu^\top(t) := \nu^\top \exp(\mathbf{Q}t)$  is typically required for one or many time intervals,  $t$ , either as a contribution to the likelihood to enable statistical inference, or to understand the evolution of the process itself. When, as in many statistical applications in, for example, epidemics, systems biology and ecology,  $\mathbf{Q}$  arises from a reaction network, or when  $\mathbf{Q}$  corresponds to a negative graph Laplacian, it is usually sparse. Building on a relatively recent development for the action of the exponential of a general sparse matrix on a vector, we use the special properties of rate matrices to create the *Single Positive Series* method, which accurately and quickly evaluates the distribution across states at a single time point in  $\mathcal{O}((r+1)\rho d)$  operations, where  $d$  is the dimension of the statespace,  $\rho = \max_{i=1,\dots,d} |Q_{ii}|$  and  $r$  is the average number of positive entries in the rows of  $\mathbf{Q}$ . We also present the *Multiple-Use Single Positive Series* algorithm which simultaneously evaluates the distribution vector at  $k$  different time points in  $\mathcal{O}((k+r)\rho d)$  operations. We demonstrate across a range of examples that the Single Positive Series method is both more accurate and more than an order of magnitude more efficient than the nearest generic and generally available competitor, and that the Multiple-Use Single Positive Series algorithm improves upon this still further.

## 1 Introduction

For many applications, statistical methods require the exponentiation of large, sparse, matrices. Such calculations are needed, for example, to evaluate the likelihood for continuous-time Markov models (e.g. Andersson and Britton, 2000) or to evaluate certain metrics for networks (e.g. Hammond et al., 2013). Standard algorithms for evaluating the matrix exponential (such as `expm` from the `Matrix` package in `R`) scale poorly with dimension,  $d$ . However, in many applications interest lies only in the action of the matrix exponential

---

\*c.sherlock@lancaster.ac.uk

on a vector; furthermore, when the matrix to be exponentiated is sparse, the calculation can be performed in  $\mathcal{O}(d)$  operations. Recently, Al-Mohy and Higham (2011) introduced an algorithm which in the vast majority of examples considered was both faster and more accurate than its competitors, but this has largely been ignored in the statistics literature. Here we present further developments of the algorithm of Al-Mohy and Higham (2011) which take advantage of the special structure of matrix exponential calculations that are common in statistics. Our key algorithm is more straightforward to implement than that of Al-Mohy and Higham (2011), yet faster, and at least as accurate, as well as being an order of magnitude faster than its nearest widely-available competitor, making accurate likelihood-based inference feasible and straightforward for systems with statespace sizes in the tens of thousands.

The exponential of a  $d \times d$  square matrix,  $\mathbf{M}$  is defined via its infinite series:  $e^{\mathbf{M}} = \sum_{i=0}^{\infty} \frac{1}{i!} \mathbf{M}^i$ . As might be anticipated from the definition, algorithms for evaluating  $e^{\mathbf{M}}$  take  $\mathcal{O}(d^3)$  operations see Moler and Van Loan (2003) for a review of many such methods. However, for a  $d$ -vector,  $v$ , the product  $e^{\mathbf{M}t}v$  is the solution to the initial value problem  $w(0) = v$ ,  $dw/dt = \mathbf{M}w$ , and is the key component of the solution to more complex differential equations such as  $dw/dt = \mathbf{M}w + \mathbf{B}u(t)$ . For this reason the numerical evaluation of the action of a matrix exponential on a vector has received considerable attention of itself (e.g. Gallopoulos and Saad, 1992; Saad, 1992; Sidje, 1998; Al-Mohy and Higham, 2011).

When  $\mathbf{M}$  is dense, evaluating

$$e^{\mathbf{M}}v = \sum_{i=0}^{\infty} \frac{1}{i!} \mathbf{M}^i v \quad (1)$$

takes  $\mathcal{O}(d^2)$  operations. However, motivated by the examples we detail in Section 1.1 our interest lies in large *sparse* matrices, and the number of operations then reduces to  $\mathcal{O}(bd)$ , where  $b$  is the average number of entries in each row of  $\mathbf{M}$ . In this case, as exemplified in the popular `Expokit` FORTRAN routines (Sidje, 1998), it is usual to estimate  $e^{\mathbf{M}}v$  via its projection on to the Krylov subspace  $\text{Span}\{v, \mathbf{M}v, \mathbf{M}^2v, \dots, \mathbf{M}^{n-1}v\}$ , where  $n \ll d$ .

With double-precision arithmetic, real numbers are stored to an accuracy of approximately  $10^{-16}$ . Thus, when a scalar,  $x$ , is very large and negative, naive numerical evaluation of the series for  $e^x$  can be innaccurate due to the cancellation of very large positive and negative terms. Evaluation of  $e^{\mathbf{M}}v$  is, typically, similarly affected, and to control these errors, algorithms for evaluating  $e^{\mathbf{M}}v$  (e.g. Sidje, 1998) use the identity

$$e^{\mathbf{M}}v = (e^{\mathbf{M}/s})^s v = e^{\mathbf{M}/s} e^{\mathbf{M}/s} \dots e^{\mathbf{M}/s} v, \quad (2)$$

where the integer  $s$  is chosen so that  $\mathbf{M}/s$  is small enough (for a suitable choice of norm) that cancellation of positive and negative terms which are ‘too large’ does not occur. The calculation on the right of (2) typically involves many more numerical operations than the direct calculation on the left and so  $s$  should be the *smallest* integer that mitigates against the cancellation of large positive and negative terms, so as to minimise the accumulation of rounding errors.

The relatively recent, ground-breaking paper Al-Mohy and Higham (2011) presents a new algorithm for evaluating the action of the exponential of a sparse matrix on a vector. Rather than reducing the dimension using Krylov subspaces and then applying standard techniques, it uses (2) directly, together with straightforward truncation of the series (1)

for  $e^{M/s}v_*$  (first with  $v_* = v$ , then with  $v_* = e^{M/s}v$  etc.). The three key contributions which make this algorithm typically both faster and more accurate than that of Sidje (1998) are detailed in Section 2.1; however, to motivate our own contribution, we briefly note two of these now. Firstly, a detailed error analysis allows for the choice of sensible values for  $s$  and the truncation point of each series,  $m$ . The process by which these values are chosen is, however, relatively complex, requiring a look-up table and other bespoke code from Al-Mohy and Higham (2009), and may relate to the reason why the only implementation we were able to find was the original `matlab` code from the authors. Secondly, the identity

$$e^M v = e^a e^{M - aI_d} v \quad (3)$$

for any scalar,  $a$ , is used to reduce the Frobenius norm of  $M$  by setting its trace to 0.

Our interest lies specifically in the left action of the exponential of a scalar multiple of the rate matrix (or infinitesimal generator),  $Q$ , of a Markov chain, on a probability vector,  $\nu$ :

$$\nu(t)^\top = \nu^\top e^{Qt} = \sum_{i=0}^{\infty} \frac{t^i}{i!} \nu^\top Q^i. \quad (4)$$

Our key observation is that, since only the diagonal elements of  $Q$  are non-positive, it is possible to shift  $Qt$  using (3) so that no elements are negative. Since probability vectors are also non-negative, all elements of all vectors in the series in (4) then become non-negative. Hence there is no cancellation of large positive and negative terms and no need to scale by a factor  $s$ . This *Single Positive Series* algorithm (SPS) reduces the number of matrix-vector operations compared to that in the algorithm of Al-Mohy and Higham (2011), typically by a factor of 3–4, concomittantly reducing the opportunities for rounding errors and speeding up the evaluation. The SPS algorithm is straightforward to implement, since  $m$  is simply a high quantile of the Poisson distribution; we do, however, provide a method for evaluating this quantile which is typically faster than standard methods. Our second contribution lies in the evaluation of (4) for multiple time points,  $t_1 < \dots < t_n$ , for example to chart the evolution of the Markov chain. These distributions are typically evaluated sequentially, since  $\nu(t_i)^\top = \nu(t_{i-1})^\top e^{Q(t_i - t_{i-1})}$ . Using the fact that, in our case,  $s = 1$ , we provide the *Multiple-Use Single Positive Series* algorithm (MUSPS) which evaluates  $\nu(t_1), \dots, \nu(t_n)$  all at once from a single evaluation of the series, rather than sequentially.

With our algorithm, or that of Al-Mohy and Higham (2011), for a Markov chain with thousands of states, evaluation of  $\nu(t)$  for values of  $t$  that see a notable change in  $\nu$  takes only a small fraction of a second, enabling direct maximum likelihood estimation of the rate parameters when the network is observed precisely at a discrete set of time points, and making Bayesian inference (via latent variables for the states at observation times) feasible for partially observed networks. As well as being faster than the algorithm of Al-Mohy and Higham (2011), the SPS algorithm is short, self-contained and straightforward to code should our `C++` implementation not fit with the user’s preferred platform. For common epidemic models in particular, the alternative statespace formulation of Ho et al. (2018) (see Section 2.2) makes Bayesian inference feasible for relatively large populations; for example, Ho et al. (2018) perform inference for the SIR model using data from the Ebola outbreak in regions of Guinea. This reduced statespace is usable, and indeed improvable, by the SPS algorithm. In systems biology and elsewhere, reaction networks often have a *countably infinite* statespace. Georgoulas et al. (2017) provides a method for dealing with

such cases using matrix exponentiation by applying the random truncation algorithm of Glynn and Rhee (2014) to the statespace itself; this method would also benefit from using the Single Positive Series algorithm, rather than the algorithm of Al-Mohy and Higham (2011).

In the remainder of this article, Section 1.1 provides several motivating examples, which will form the basis of the numerical comparisons of SPS and MUSPS against competitors in Section 4. Section 2 provides further background on the algorithm of Al-Mohy and Higham (2011) and aspects of the algorithm of Ho et al. (2018), whilst the SPS and MUSPS algorithms themselves are detailed in Section 3.

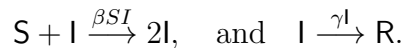
## 1.1 Examples and motivation

Both by way of motivation and because we shall use them later to illustrate our method, we now present three examples of continuous-time Markov processes, and one example motivated by networks, where a finite, sparse rate matrix contains all of the information about the dynamics.

For each Markov process, the set of possible states can be placed in one-to-one correspondence with a subset of the non-negative integers  $\{1, \dots, d\}$ . The off-diagonal elements of the rate matrix,  $\mathbf{Q}$ , are all non-negative, and the  $i$ th diagonal element is  $Q_{ii} = -\sum_{j=1, j \neq i}^d Q_{i,j}$ . A chain that is currently in state  $i$  leaves this state upon the first event of a Poisson process with a rate of  $-Q_{i,i}$ ; the state to which it transitions is  $j$  with a probability of  $Q_{i,j}/(-Q_{i,i})$ . Whilst the rate matrix,  $\mathbf{Q}$ , is a natural description of the process, the likelihood for typical observation regimes involves the transition matrix,  $e^{\mathbf{Q}t}$ , the  $i, j$ th element of which is exactly  $\mathbb{P}(X_t = j | X_0 = i)$ .

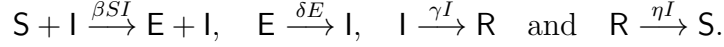
Given a network, or graph  $\mathcal{G}$  with  $d$  vertices (or nodes), the adjacency matrix,  $A$  is the  $d \times d$  matrix with  $A_{ii} = 0$  and, for  $i \neq j$ , if nodes  $i$  and  $j$  are connected then  $A_{ij}$  is some positive weight representing the strength of the connection, else  $A_{ij} = 0$ . The graph Laplacian is  $L = D - A$ , where  $D$  is the diagonal matrix with  $D_{ii} = \sum_{j=1}^d A_{i,j}$ . The negative Laplacian,  $-L$ , has the same properties as a rate matrix and, as we shall see in Example 4, this connection can be related to certain key properties of a graph.

**Example 1. The SIR model for epidemics.** The SIR model for a disease epidemic has 3 ‘species’: those who are susceptible to the epidemic,  $S$ , those both infected and infectious,  $I$ , and those who have recovered from the epidemic and play no further part in the dynamics,  $R$ . The non-negative counts of each species are denoted by  $S$ ,  $I$ , and  $R$ . For relatively short epidemics the population,  $n_{pop}$ , is assumed to be fixed, and so the state of the Markov chain, represented by  $(S, I)$ , is subject to the additional constraint of  $S + I \leq n_{pop}$ . The two possible reactions and their associated rates are:



**Example 2. The SEIRS model for epidemics.** The SEIRS epidemic model starts from the SIR model and inserts an additional state of infected but not yet infectious,  $E$  (‘exposed’). The number of these individuals is denoted by  $E$  and the state  $(S, E, I)$  is subject to the constraint that  $S + E + I \leq n_{pop}$ . Removed subjects also gradually lose their

immunity so that the reactions are:



**Example 3. The Moran model for allele frequency** describes the time evolution of the frequency of two alleles,  $A_1$  and  $A_2$  in a population with a fixed size of  $n_{pop}$ . Individuals with allele  $A_1$  reproduce at a rate of  $\alpha$ , and those with  $A_2$  reproduce at a rate of  $\beta$ . When an individual dies it is replaced by the offspring of a parent chosen uniformly at random from the whole population (including the individual that dies). The allele that the parent passes to the offspring usually matches its own, however as it is passed down an allele may mutate; allele  $A_1$  switching to  $A_2$  with a probability of  $u$ , and  $A_2$  switching to  $A_1$  with a probability of  $v$ . Let  $X$  be the number of individuals with allele  $A_1$ . The two reactions are



Setting  $f_N = X/n_{pop}$ , the corresponding infinitesimal rates are

$$\lambda_N = (1 - f_N) [\alpha f_N (1 - u) + \beta (1 - f_N) v] \quad \text{and} \quad \mu_N = f_N [\beta (1 - f_N) (1 - v) + \alpha f_N u],$$

where the unit of time is the expectation of the exponentially distributed time for an individual to die and be replaced.  $\square$

Our fourth example provides a characterisation of the discrepancy between two graphs in terms of the transmission of information. Given two graphs,  $\mathcal{G}_1$  and  $\mathcal{G}_2$  with the same vertices but different edges (e.g. representing different observations of the connections, possible imputations given incomplete information, or observations of two different types of connections), and Laplacians  $L_1$  and  $L_2$ , Hammond et al. (2013) defines the *graph diffusion distance* between  $\mathcal{G}_1$  and  $\mathcal{G}_2$  as:

$$\xi(\mathcal{G}_1, \mathcal{G}_2; t) := \|\exp(-L_1 t) - \exp(-L_2 t)\|_{fr},$$

where  $\|\cdot\|_{fr}$  is the Frobenius norm. The idea is that two graphs might be deemed similar if they enable similar patterns of information transmission. The negative Laplacian is a rate matrix, and the  $i$ th row of  $\exp(-Lt)$  represents the distribution over the network after time  $t$  of a unit of information that was placed on node  $i$  at time 0. The Frobenius norm, therefore, represents an average over all possible initial starting nodes of the  $L_2$  discrepancies in the time- $t$  distributions.

Calculating and storing the full matrix exponential for a set of large graphs is prohibitive both in computational time and storage space; moreover, some initial conditions will be of much more interest than others.

**Example 4. Random graphs** Given a particular, shared initial distribution across nodes,  $\nu$ , the evolution of the discrepancy between the probability distributions can provide a useful measure of the difference in the transmission properties of the graphs. We have:

$$d_\nu(\mathcal{G}_1, \mathcal{G}_2; t) := \|\nu^T \exp(-L_1 t) - \nu^T \exp(-L_2 t)\|_1. \quad (5)$$

$\square$

Other examples of finite reaction networks include the dimerisation reactions and the Michaelis-Menten reaction kinetics (e.g. Wilkinson, 2012) and other epidemic models such as the SEIR and SIRS models (e.g. Andersson and Britton, 2000).

## 2 Further Background

Redefining  $Q \leftarrow Qt$ , we require  $\mu^\top = \nu^\top e^Q$ , where  $\mu$  and  $\nu$  are probability  $d$ -vectors and  $Q$  is a  $d \times d$  rate matrix for a reaction network. We now detail the algorithm of Al-Mohy and Higham (2011) and summarise the key numerical results from that article. We then briefly describe the alternative statespace formulation for epidemic models, from Ho et al. (2018).

### 2.1 The algorithm of Al-Mohy and Higham

As stated in the introduction the algorithm presented in Al-Mohy and Higham (2011), which we, henceforth refer to as AMH, uses simple series truncation to evaluate  $e^{Mt}v$  using the decomposition in (2). AMH benefits from three key contributions. Firstly, an error analysis allows for sensible choices of  $s$  and the value,  $m$ , at which the Taylor series should be truncated; more detail on this is given below. Secondly, the identity (3) is used to reduce the Frobenius norm of  $M$  by setting its trace to 0. Finally, the evaluation of each series for  $e^{M/s - a/sI_d}v_*$  is truncated early, at the  $k$ th term, if the sum of the sizes of the two most recent terms,  $\|A^{k-1}v_*\|_1/(k-1)! + \|A^k v_*\|_1/k!$  (where  $A = (M - a)/s$ ), is less than the product of some tolerance and the size of the partial sum,  $\|\sum_{j=0}^k A^j v_*/j!\|_1$ . This leads to a problem-specific speed up which can be substantial.

When  $e^{Mt}v$  is required for multiple time points,  $t_1, \dots, t_n$ , the natural procedure is to calculate  $v(t_1) = e^{Mt_1}v$  and then  $e^{M(t_2-t_1)}v(t_1)$  etc. However, when the set of time points is dense this can lead to a large accumulation of rounding errors. AMH reduces the build up of rounding errors by using, for example,  $e^{Mt_2}v$  whenever there would be no additional computational cost over using  $e^{M(t_2-t_1)}v(t_1)$ .

The complexity of the AMH algorithm, and perhaps the reason why we could only find it in the authors' original `matlab` code, lies in the calculation of appropriate values for  $m$  and  $s$ , which, in particular, requires further, bespoke `matlab` code (by the same authors) for approximating the induced  $L_1$  norm of a matrix (and its powers) using one or several matrix-vector multiplications for each power. With the hyper parameters for the algorithm given by the authors and hard-coded into the `matlab` code, except when the approximation of  $\|M\|$  is found to be sufficiently small with 'sufficient' depending on the error tolerance chosen (double or single),  $\|M^p\|$  is required for each  $p$  between 1 and 9, and each of these is approximated using a single matrix-vector multiplication.

In Al-Mohy and Higham (2011) the new algorithms are compared against many competitors across a very wide variety of examples. Whilst they do not dominate all other algorithms across all examples, against a given competitor the relevant new algorithm is both more accurate and faster in the vast majority of cases. In particular, the single-time algorithm is found to be both more accurate and typically between 2 and 22 times faster than `expv`. On the only occasion when the new algorithm is found to be slower than `expv` the relative slow down is due to the matrix norm estimation, which is not required by SPS.

## 2.2 Birth formulation of the SIR and SEIR processes

Ho et al. (2018) reformulate the SIR and SEIR models in terms of births of the E (for SEIR only), I and R species. A recursive formula for the Laplace transform of the transition probability to a given new state in terms of transition probabilities for old states then permits estimation of the transition vector from a known initial starting point in  $\mathcal{O}(d)$  operations, where  $d$  is the dimension of the statespace. When exact observations are available, the size of the statespace can then be reduced dramatically.

Consider, first, an SIR model with observations of  $(S_0, I_0)$  and  $(S_1, I_1)$  at times of 0 and 1. The number of I births is  $n_I = S_0 - S_1$ , and the number of R births is  $n_R = S_0 + I_0 - (S_1 + I_1)$ . The total size of the statespace of possible events given the observations is therefore  $d_{SIR} := n_I n_R$ . For an SEIR model a similar argument leads to a product of the number of births of E, I and R.

We may use the same statespace formulation as Ho et al. (2018), provided we include an additional coffin state, C, with  $Q_{C,j} = 0$  for all  $j = \{1, \dots, d\} \cup C$ . Any births that would leave the statespace (and hence contradict the observation at time 1) instead go to C.

## 3 New algorithms

Given a vector  $\nu$ , a matrix  $Q$  and a precision  $\epsilon > 0$ , the *Single Positive Series* (SPS) algorithm estimates  $\mu^\top = \nu^\top e^Q$ , whilst the *Multiple-Use Single Positive Series* (MUSPS) algorithm estimates  $\nu(t_1)^\top = \nu^\top e^{Qt_1}, \dots, \nu(t_n)^\top = \nu^\top e^{Qt_n}$  for a sequence of times  $t_1 < \dots < t_n$ . Unlike any previous algorithms, however, both the SPS and MUSPS algorithms operate by truncating a single series none of whose terms can be negative, rather than truncating multiple series where terms may change sign. Given an  $\epsilon > 0$ , our algorithms calculate  $\hat{\mu}$  such that the (guaranteed to be non-negative) *true* missing probability mass in each of the  $d$  dimensions is controlled:

$$0 < 1 - \sum_{i=1}^d \hat{\mu}_i^* < \epsilon \quad \text{and} \quad 0 < 1 - \sum_{i=1}^d \hat{\nu}(t_j)_i^* < \epsilon \quad (j = 1, \dots, n),$$

where  $\hat{\mu}^*$  and  $\hat{\nu}(t_j)^*$  are the probability vectors that would be calculated if there were no rounding errors, and the only errors were due to the truncation of the infinite series. Typically we aim for the error to be similar to the machine's precision. We control the absolute truncation error since with any truncation of the power series it is impossible to obtain general control of the *relative* error in a given component of  $\mu$ ,  $|\hat{\mu}_i/\mu_i - 1|$ . Consider, for example, a Moran process (Example 3), where the  $Q$  matrix is tridiagonal. Then  $Q^k$  is also banded, with a band width of  $2k + 1$ . For any given  $m_{max}$ , and  $\nu = (1, 0, 0, \dots)$ , set  $d > m_{max} + 1$ . The truncated approximation to  $e^Q$  gives a transition probability of 0 for all states above  $m_{max} + 1$ , yet, in truth there is a non-zero probability of such a transition.

### 3.1 The Single Positive Series algorithm

Let

$$\rho := \max_{i=1,\dots,d} |Q_{ii}| \quad \text{and} \quad P = (1/\rho)Q + I. \quad (6)$$

$P$  is a Markov transition matrix. However,  $e^Q = e^{\rho P - \rho I} = e^{-\rho} e^{\rho P}$ . Thus

$$\mu^\top = \nu^\top e^Q = e^{-\rho} \nu^\top \sum_{i=0}^{\infty} \frac{\rho^i}{i!} P^i \approx e^{-\rho} \sum_{i=0}^m \frac{\rho^i}{i!} \nu^\top P^i =: \hat{\mu}^{*\top}.$$

Since no element of  $\nu$  or  $P$  is negative, there is no possibility for cancellation of terms of opposite sign. Now

$$\sum_{i=1}^d \hat{\mu}_i^* = \hat{\mu}^{*\top} \mathbf{1} = e^{-\rho} \sum_{i=0}^m \frac{\rho^i}{i!} \nu^\top P^i \mathbf{1} = e^{-\rho} \sum_{i=0}^m \frac{\rho^i}{i!}.$$

So the absolute relative error, or missing probability mass, due to truncation is

$$r_m(\rho) := e^{-\rho} \sum_{i=m+1}^{\infty} \frac{\rho^i}{i!},$$

the tail probability of a  $\text{Poisson}(\rho)$  random variable. Of direct interest to us is

$$m_\epsilon(\rho) := \inf\{m \in \mathbb{N} : r_m(\rho) \leq \epsilon\},$$

the smallest  $m$  required to achieve an error of at most  $\epsilon$ , or, essentially, the quantile function for a  $\text{Poisson}(\rho)$  random variable, evaluated at  $1 - \epsilon$ . Theorem 1, which is proved in Appendix A, provides relatively tight bounds on  $m_\epsilon(\rho)$  for any  $\rho$  and  $\epsilon$  that might be used.

**Theorem 1.** *If  $1 - e^{-\rho} \leq \epsilon$ ,  $m_\epsilon(\rho) = 0$ , and if  $\rho \leq \epsilon^{1/2}$ ,  $0 \leq m_\epsilon(\rho) \leq 1$ . More generally:  $m_\epsilon(\rho) \leq \lceil m_+ \rceil$ , where*

$$m_+ := \rho - \frac{1}{3} \log \epsilon \left\{ 1 + \left( 1 - \frac{18\rho}{\log \epsilon} \right)^{1/2} \right\} - 1. \quad (7)$$

Furthermore,

$$\lfloor m_- \rfloor \leq m_\epsilon(\rho) \leq \lceil m_{++} \rceil,$$

where both inequalities require  $\epsilon < 0.04$  and the latter also requires  $1 - e^{-\rho} > \epsilon$  and  $B > \log \epsilon$ , where

$$m_- := \rho + \{2\rho\}^{1/2} \left\{ -\log(\epsilon\sqrt{2\pi}) - \frac{3}{2} \log A + \log(A-1) \right\}^{1/2}, \quad (8)$$

$$m_{++} := \rho + \frac{B - \log \epsilon}{3} \left\{ 1 + \left( 1 + \frac{18\rho}{B - \log \epsilon} \right)^{1/2} \right\}, \quad (9)$$

$$A := 2\rho h\left(\frac{m_+ + 1}{\rho}\right), \quad B := -\frac{1}{2} \log 4\pi\rho h\left(\frac{m_-}{\rho}\right),$$

and  $h(x) = x - 1 + x \log x$ .



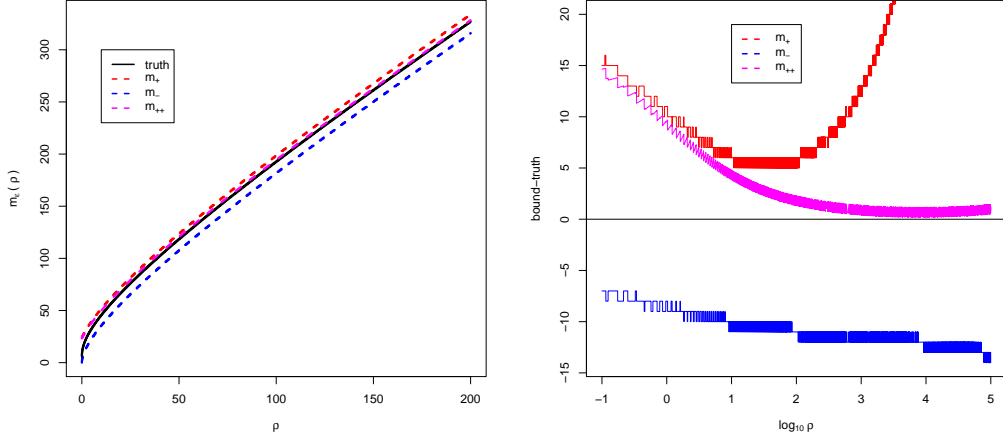


Figure 1: Left panel:  $m_\epsilon(\rho)$  together with its upper and lower bounds from Theorem 1, plotted against  $\rho$  for  $\epsilon = 10^{-16}$ . Right panel  $\text{bound}(\rho) - m_\epsilon(\rho)$  against  $\log_{10} \rho$  for  $\epsilon = 10^{-16}$ .

The bound (7) arises from a standard argument, whereas those in (8) and (9) are derived from extremely sharp but intractable bounds on  $r_m(\rho)$  in Short (2013); our bounds use only elementary functions and so are much quicker to compute than the quantile upper bound in Short (2013), yet from Figure 1 they are still very sharp. The bounds in (8) and (9) together with the alternative form in (10) permit a simple but fast binary search for  $m_\epsilon(\rho)$  (see also Section 3.4). Equation (10) follows from the equivalence between at least  $m + 1$  events of a Poisson process with a unit rate occurring by time  $\rho$  and the time until the  $m + 1$ th event being at most  $\rho$ :

$$r_m(\rho) = \frac{1}{\Gamma(m+1)} \int_0^\rho x^m e^{-x} dx. \quad (10)$$

As well as providing a tight strict upper bound on the number of sparse vector-matrix multiplications required by our algorithm, the bounds lead directly to the following asymptotic cost:

**Corollary 1.** *For any fixed error tolerance,  $\epsilon$ ,  $\lim_{\rho \rightarrow \infty} m_\epsilon(\rho)/\rho = 1$ .*

The Single Positive Series (SPS) algorithm is presented as Algorithm 3.1. For large values of  $\rho$ , although there is no problem with large positive and negative terms cancelling, it is possible that the partial sum  $\sum_{i=0}^k \frac{\rho^i}{i!}$  might exceed the largest floating point number storable on the machine. Our algorithm circumvents this problem by occasionally renormalising the vector partial sum when the most recent contribution is large, and compensating for this at the end; see lines 5, 12 and 14. One could, alternatively, renormalise when the partial sum itself becomes large, but the translation of the algorithm to multiple time points (Section 3.3) becomes both messier and computationally slower, with no benefits for the accuracy of the algorithm for any  $\rho$  values for which the algorithm might feasibly be used.

---

**Algorithm 1** Single Positive Series algorithm for  $\nu^\top e^Q$  with a missing mass of at most  $\epsilon$ .

---

```

1:  $\rho \leftarrow \max_{i=1}^d |Q_{i,i}|$ ;  $P \leftarrow Q + \rho I_d$ ;  $BIG \leftarrow 10^{100}$ .
2: Find  $m_\epsilon(\rho)$ .
3:  $b \leftarrow \|\nu\|_1$ ;  $c \leftarrow 0$ .
4: if  $b > BIG$  then
5:    $\nu \leftarrow \nu/b$ ;  $c \leftarrow c + \log b$ ;  $b \leftarrow 1$ .
6:  $v_{pro} \leftarrow v_{sum} \leftarrow \nu$ .
7:  $f \leftarrow 1$ .
8: for  $j$  from 1 to  $m$  do
9:    $v_{pro}^\top \leftarrow v_{pro}^\top P/f$ ;  $b \leftarrow b * \rho/f$ .
10:   $v_{sum} \leftarrow v_{sum} + v_{pro}$ .
11:  if  $b > BIG$  then
12:     $v_{pro} \leftarrow v_{pro}/b$ ;  $v_{sum} \leftarrow v_{sum}/b$ ;  $c \leftarrow c + \log b$ ;  $b \leftarrow 1$ .
13:   $f \leftarrow f + 1$ .
14: return  $e^{c-\rho} \times v_{sum}$ .
```

---

## 3.2 Options

We now describe two optional extensions to the SPS algorithm: renormalisation and two-tailed truncation.

Since  $S := \sum_{i=1}^d \nu_{t,i} = \sum_{i=1}^d \nu_{0,i}$  there is no need to keep track of the logarithmic offset ( $c$  in Algorithm 3.1). Instead the final vector ( $v_{sum}$  in Algorithm 3.1) is renormalised at the end so that its components sum to  $S$ . Renormalisation when a rate matrix is being exponentiated is included as an option in `expoRkit` (Sidje, 1998), for example. In experiments detailed in Section 4.1 and 4.2 we find that it improves the accuracy of the algorithm by between a factor of 2 and several orders of magnitude at no additional computational cost.

In contrast to the general applicability of renormalisation, two-tailed truncation is unique to the SPS algorithm and reduces the computational cost with no loss of accuracy. When  $\rho$  is moderate or large, the total mass of probability from the initial value of  $v_{sum}$  and the early values accumulated into  $v_{sum}$  (Steps 6 and 10 of Algorithm 3.1) is negligible (has a relative value smaller than  $\epsilon/2$ , say) compared with the sum of the later values. In such cases  $v_{sum}$  may be initialised to 0 and step 10 omitted for values of  $j$  beneath some  $m_{lo}$ . Proposition 1 (see Appendix B for the proof) shows that if  $m$  is chosen such that  $\mathbb{P}(\text{Po}(\rho) > m) \leq \epsilon/2$  then setting  $m_{lo} := \max(0, 2\lfloor \rho - 0.5 \rfloor - m)$  ensures that the missing probability mass is no more than  $\epsilon$ . For large  $\rho$ ,  $m - m_{lo} = \mathcal{O}(\sqrt{\rho})$ , so with two-tailed truncation the cumulative cost of Step 10 dwindles compared with the other  $\mathcal{O}(d)$  costs, all of which are repeated  $\mathcal{O}(\rho)$  times.

**Proposition 1.** *Given  $\rho > 0$ , let  $p_n = e^{-\rho} \rho^n / n! = \mathbb{P}(\text{Poisson}(\rho) = n)$ , and let  $c = \lfloor \rho - 1/2 \rfloor$ . Then for  $a \leq c - 1$ ,  $\sum_{j=0}^{c-a-1} p_j < \sum_{j=c+a+1}^{\infty} p_j$ .*

### 3.3 The Multiple-Use SPS algorithm

The SPS algorithm evaluates  $e^{Qt}$  for a single time,  $t$ . Suppose, now, that transitions for multiple time points,  $t \in \mathcal{T}$ , are required. We use the identity

$$\nu^\top e^{Qt} = e^{-\rho t} \nu^\top e^{\rho P t} = e^{-\rho t} \sum_{i=0}^{\infty} \left( \frac{t}{t_*} \right)^i \times \frac{\rho^i t_*^i}{i!} \nu^\top P^i,$$

where  $P$  is as defined in (6), and  $t_* > 0$ .

Then, with  $\rho$ ,  $b$  and  $\nu_{pro}$  as in Algorithm 3.1, for each additional time interval,  $t \in \mathcal{T}$ , since  $\rho(t) = \rho t$ , we initialise  $m(t) = m(\rho t, \epsilon)$ . Within the iterations, we update  $\nu_{pro}$  and  $b$  as in Algorithm 3.1 but for some relevant  $t_*$  (rather than  $t_* = 1$ ) and, effectively, include the additional step for each  $t$ :  $v_{sum}(t) \leftarrow v_{sum}(t) + (t/t_*)^{j+1} \nu_{pro}$ . We, therefore, avoid the potential build up of errors from partitioning the total time interval into  $|\mathcal{T}| > 1$  sub-intervals. Furthermore, we reduce the cost since the vector-matrix multiplication, which involves  $d(n_r + 1)$  multiplications and additions is only performed once for each  $j$ ; for all times  $t < 1$ , the only  $\mathcal{O}(d)$  update is to  $v_{sum}(t)$ , and this involves a single addition and division. Moreover, although the loop over  $j$  is repeated  $m(\rho, \epsilon)$  times, for any given  $t$ ,  $v_{sum}(t)$  is only updated when the contribution to the eventual total would be non-negligible.

Both renormalisation and two-tailed truncation can be applied to the MUSPS algorithm if desired, and the algorithm with both of these options (MUSPS2r) typically provides the best combination of speed and accuracy. The bare bones of MUSPS2r is provided in Algorithm 3.3; for simplicity of presentation the version does not deal with numerical underflow or overflow, and the necessary additional steps are provided in Appendix C.

### 3.4 Implementation details

C++ code for SPS and MUSPS together with some working examples is (for now) besides the link to this paper at <https://www.maths.lancs.ac.uk/~sherloc/Publications/publications.html>

For a single time point, our binary search algorithm homes in on the required  $m$  using the upper and lower bounds of Theorem 1 together with the identity (10), the right hand side of which can be evaluated quickly and accurately using the standard C++ toolbox, **boost**. This is quicker than the standard implementation of the Poisson quantile function (e.g. as implemented in **boost**), which uses the Cornish-Fisher expansion to approximate the quantile, hence needing an expensive evaluation of  $\Phi^{-1}$ , and then conducts a local search. When evaluating  $\nu^\top e^{Qt}$  for multiple times  $t_1, \dots, t_n$ , presented in ascending order, our function can be speeded up still further for  $j$  in  $2, \dots, n$  by using  $m_\epsilon(\rho t_{j-1})$  as a lower bound for  $m_\epsilon(\rho t_j)$ .

The speed of a vector multiplication by a sparse-matrix depends on the implementation of the sparse matrix algorithm. In R (R Core Team, 2018) and in C++ **Armadillo** (Sander-son and Curtin, 2016, 2018), sparse matrices are stored in column-major order. Hence pre-multiplication of the sparse matrix by a vector,  $\nu^\top Q$ , is much quicker than post multiplication,  $Q\nu$ . In other languages, such as **Matlab**, sparse matrices are stored in row-major

---

**Algorithm 2** MUSPS2r essentials for  $\nu^\top e^{\mathbf{Q}t_i}$  with  $t_1 < \dots < t_n$  and missing mass  $\leq \epsilon$ .

---

```

1:  $\rho \leftarrow \max_{i=1}^d |Q_{i,i}|$ .
2:  $P \leftarrow Q + \rho I_d$ .
3: Find  $m_i^{hi} := m_{\epsilon/2}(\rho t_i)$  and  $m_i^{lo}(\rho; m_i^{hi})$  ( $i = 1, \dots, n$ ). ▷ two-tailed truncation points
4:  $b_{start} \leftarrow b \leftarrow \|\nu\|_1$ ;  $m_{max} \leftarrow m_n^{hi}$ ;  $m_{n+1}^{lo} = m_{max} + 1$ .
5:  $\nu_{pro} \leftarrow \nu$ ;  $\nu_{sum,i} \leftarrow \underline{0}$ ,  $g_i = 1$  ( $i = 1, \dots, n$ ).
6:  $i \leftarrow 0$ .
7: while  $m_i^{lo} == 0$  do
8:    $\nu_{sum,i} = \nu_{pro}$ .
9:    $i \leftarrow i + 1$ 
10:  $i_{hi} \leftarrow i - 1$ ;  $i_{lo} \leftarrow 0$ ;  $j \leftarrow 1$ ;  $f \leftarrow 1$ .
11: while  $j \leq m_{max}$  do
12:   while  $m_{i_{hi}+1}^{lo} \leq j$  do
13:      $i_{hi} \leftarrow i_{hi} + 1$ . ▷  $i_{hi}$  is last relevant time for  $j$ 
14:   while  $m_{i_{lo}+1}^{hi} < j$  do
15:      $i_{lo} \leftarrow i_{lo} + 1$ . ▷  $i_{lo}$  is first relevant time for  $j$ 
16:    $\nu_{pro} \leftarrow \nu_{pro} P$ ;  $b \leftarrow \rho b$ .
17:   if  $i_{hi} > 0$  then  $\nu_{pro} \leftarrow (t_{i_{hi}}/f)\nu_{pro}$ ;  $b \leftarrow b t_{i_{hi}}/f$ . ▷ size for current largest  $t$  only
18:    $g_i = g_i \times t_i/t_{i_{hi}}$  ( $i = i_{lo}, \dots, i_{hi}$ ).
19:    $\nu_{sum,i} \leftarrow \nu_{sum,i} + g_i \nu_{pro}$  ( $i = i_{lo}, \dots, i_{hi}$ ). ▷ only update for times between  $i_{lo}$  and  $i_{hi}$ 
20:    $f \leftarrow f + 1$ ;  $j \leftarrow j + 1$ .
21:  $v_{sum,i} \leftarrow b_{start} \nu_{sum,i} / \|\nu_{sum,i}\|_1$  ( $i = 1, \dots, n$ ). ▷ renormalise
22: return  $v_{sum,1,\dots,n}$ .
```

---

order and post-multiplication is the quicker operation, so  $Q^\top$  should be stored and used, rather than  $Q$ .

## 4 Numerical comparisons

In Al-Mohy and Higham (2011) the new algorithm (henceforth referred to as AMH) is compared across many examples against state-of-the-art competitors, including, in particular, the `expokit` function `expv` (Sidje, 1998). In most of the experiments, for single times and multiple time points, AMH is found to give comparable or superior accuracy together with superior computational speed. Given these existing comparisons and that comparing direct timings of algorithms coded in different languages confounds the efficiencies of the algorithms and of the compilers, we perform a relatively short comparison of accuracy and clock time between SPS, `expv` and a bespoke algorithm for epidemic processes, before comparing SPS and AMH in terms of accuracy and computational complexity across a range of examples. We then move on to multiple time points and exhibit additional gains in both speed in accuracy, via the MUSPS algorithm.

The highest accuracy available in C++ using sparse matrices and the `armadillo` linear algebra library is double precision, which we used throughout in our implementation of both our algorithm and that of Al-Mohy and Higham (2011). For the SPS algorithm we consider two settings:  $\epsilon = 10^{-9}$  (for accuracy comparable with the algorithm of Ho et al. (2018); see Section 2.2) and  $\epsilon = 10^{-16}$ , where the missing probability mass is just below the available precision. For the SPS algorithm, following the four options in Section 3.2; the label ‘r’ indicates that renormalisation was used and the label ‘2’ indicates that two-tailed truncation was used.

### 4.1 Comparison with state-of-the art algorithms other than AMH

We consider the collection (see the first three rows of Table 1) of  $(S, I)$  (susceptible and infected) values for the Eyam plague that originated in Raggett (1982) and were used in Ho et al. (2018) to examine the speed and accuracy of the algorithm for the birth representation of the SIR model briefly described in Section 2.2. We set the parameters to their maximum-likelihood estimates,  $(\beta, \gamma) = (0.0196, 3.204)$  and consider the likelihood for the data in Table 1. In addition, to mimic the size of potential changes between observation times and the size of the elements of the rate matrix from a larger population, we also evaluated the likelihood for the jump directly from the data at time 0 to the data at time 4. The final two rows of Table 1 refer to the rate matrix for the transition between consecutive observations and provide the dimension the matrix and the absolute value of its largest entry ( $\rho$ ).

For the SPS algorithm, with  $\epsilon = 10^{-9}$  and  $10^{-16}$ , the algorithm of Ho et al. (2018) and the FORTRAN routine `expv` from the `expokit` package (Sidje, 1998) we found the CPU time for 1000 estimations of the likelihood (100 estimates for the likelihood for the jump from  $t = 0$  to  $t = 4$ ); each experiment was performed three times, and the range of timings is given. We also recorded the error in the evaluation of the log likelihood. Given that the true likelihood is not known, the error using SPS with  $\epsilon = 10^{-16}$  was approximately bounded

Table 1: Time (in units of 31 days), and numbers of susceptibles and infecteds, originally from Raggett (1982). The final rows indicates, for each pair of consecutive observations, the size of the statespace for evaluating the transition probability and the  $\rho$  value for the associated rate matrix.

Time	0	0.5	1.0	1.5	2.0	2.5	3.0	4.0	0.0-4.0
S	254	235	201	153	121	110	97	83	
I	7	14	22	29	20	8	8	0	
$d$	-	261	946	2059	1387	289	197	346	30789
$\rho$	-	101.5	171.4	217.1	170.1	83.1	53.6	106.3	3439.5

Table 2: Timings for estimating the full log-likelihood (1000 repeats) and the log-likelihood for the jump from the initial to the final observation (100 repeats), for the Eyam data set, together with the accuracies of the estimates. \* **expv** used all 8 cores on the machine at 100% capacity, whereas HCS and SPS both used only 1 core at 100%.

Algorithm	Full likelihood		Jump likelihood	
	Time (secs)	Accuracy	Time (secs)	Accuracy
HCS	47.98–48.00	$5.7 \times 10^{-8}$	48.29–48.42	$4.3 \times 10^{-9}$
<b>expv</b>	37.02–37.05*	$1.2 \times 10^{-13}$	129.40–130.53*	$4.7 \times 10^{-12}$
SPS( $10^{-9}$ )	14.61–14.66	$8.5 \times 10^{-9}$	91.48–91.53	$1.3 \times 10^{-9}$
SPSr( $10^{-9}$ )	14.61–14.69	$3.4 \times 10^{-9}$	91.48–91.64	$3.3 \times 10^{-10}$
SPS2( $10^{-9}$ )	14.59–14.71	$5.1 \times 10^{-9}$	86.23–86.29	$6.9 \times 10^{-10}$
SPS2r( $10^{-9}$ )	16.59–14.69	$2.6 \times 10^{-9}$	86.18–86.53	$1.2 \times 10^{-10}$
SPS2r( $10^{-16}$ )	16.44–16.52	$< 1 \times 10^{-15}$	89.66–89.75	$< 1 \times 10^{-14}$

by examining the discrepancy from the result produced by AMH with  $(s, m)$  chosen for double-precision arithmetic.

The results are presented in Table 2. Since using renormalisation and two-tailed truncation together produced the fastest and most accurate evaluations, we only considered this combination when using  $\epsilon = 10^{-16}$ . When using **expv** we did not include the (considerable) cost of creating the sparse rate matrix for each transition, since this was necessarily performed in R. The timings for the SPS algorithm do, however, include matrix-creation costs, which accounted for around 1% of the total cost.

As will be discussed further in Section 4.2, the choice of tolerance,  $\epsilon$ , typically has only a small effect on the speed of SPS. For the full likelihood evaluation, SPS( $\epsilon = 10^{-9}$ ) is over 3 times as fast as HCS and more accurate. The more accurate SPS( $\epsilon = 10^{-16}$ ) is roughly 3 times faster than HCS as well as being more accurate even than **expv** and over twice as fast as **expv**; however this timing does not take into account that **expv** was using eight times the processor power of the other algorithms (**expv** is automatically optimised to the machine on which it is compiled, and attempting to restrict it to a single core caused it to slow down by a factor of 300, rather than 8). This factor also does not account for the fact that **FORTRAN** is known to deal more efficiently with matrices than does C or C++ (e.g. <https://modelingguru.nasa.gov/docs/DOC-2625>).

For the single large jump between observations, we see the same pattern in terms of ac-

curacy. The gain in efficiency by using two-tailed-truncation is larger because  $\rho$  is larger ( $m_{lo} = 3081$  and  $m = 3797$ ), but despite this, HCS is now more efficient than SPS, although considerably less accurate than SPS ( $\epsilon = 10^{-16}$ ). However, in addition to the savings in state-space size made by Ho et al. (2018), further savings, are possible for SPS and `expv`. For example, for the SIR model, the constraint that:  $I(t) \geq 0$  implies that  $n_R(t) \leq I_0 + n_I(t)$ . For the single big observation jump this gives that  $n_R(t) \leq 7 + n_I(t)$ , almost halving the number of states that need to be considered. With this saving, SPS would be of a similar speed to HCS. Analogous savings of up to a factor of 6 would be possible for an SEIR model.

We consider a further example, Example 5, chosen for tractability so that the  $\nu$  values can be calculated using greater precision and the true errors ascertained.

**Example 5. Immigration-death** A single species has  $X$  members in a confined space with  $n$  available slots. The species dies out with a rate proportional to the current frequency, and immigration occurs with a rate proportional to the number of empty slots.

$$X \xrightarrow{\mu X} \emptyset \quad \text{and} \quad \emptyset \xrightarrow{\gamma(n-X)} X.$$

Transition probabilities from  $X(0) = n$  are derived in Appendix D. □

Setting  $X(0) = n = 1000$ ,  $\mu = 0.05$ ,  $\gamma = 0.01$  and  $t = 20$ , we timed 1000 calculations of the probability vector  $\hat{\nu}(t)$  and examined  $\|\hat{\nu}(t) - \nu^{true}(t)\|_1$ . Using 8 cores at 100%, `expv` took 43.0 seconds, with an error discrepancy of  $1.0 \times 10^{-11}$ , whereas on a single core, SPS2r ( $\epsilon = 10^{-16}$ ) took 12.8 seconds with a discrepancy of  $8.5 \times 10^{-16}$ ; the accuracy of SPSr was almost identical, whereas the discrepancies of both SPS and SPS2 were  $1.2 \times 10^{-14}$ ; the timings were all within 3% of that of SPS2r, which was the quickest. We then repeated the experiment but with  $n = 10000$  and 100 repetitions. Using 8 cores at 100%, `expv` took 301.5 seconds, with an accuracy of  $2.8 \times 10^{-11}$ , whereas using a single core, SPS2r ( $\epsilon = 10^{-16}$ ) took 108.9 seconds with an accuracy of  $3.4 \times 10^{-15}$  (SPS2r/SPSr) and  $1.5 \times 10^{-12}$  (SPS/SPS2).

Even allowing for a reduction in efficiency because of communication costs between cores, the results for the immigration-death model and those from Table 2 suggest that SPS is at least an order of magnitude faster than its nearest generic and easily available competitor, `expv` from `expoRkit`, as well as several orders of magnitude more accurate.

## 4.2 Comparison with the algorithm of Al-Mohy and Higham

We now compare the computational complexity and the accuracy of our method and that of Al-Mohy and Higham (2011) across four reaction networks. Complexity is measured in terms of  $n_{sparse}$ , the number of (sparse) vector-matrix multiplications required in evaluating  $e^{Qt}$ . The first example is chosen specifically because its transition probabilities are tractable and exact  $L_1$  errors in the transition probability vectors can, therefore, be provided. Since an absolute truth is not available for the second and third examples, for a transition of time  $t$  from the initial condition, accuracy for these examples is indicated by the absolute discrepancy in the probability vector:  $\|\widetilde{\nu^\top e^{Qt}} - \widehat{\nu^\top e^{Qt}}\|_1$ , where  $\widetilde{a}$  and  $\widehat{a}$  represent two different estimates of the vector  $a$ . We refer to the double and single precision error tolerance

settings for the algorithm of Al-Mohy and Higham (2011) as AMHd and AMHs respectively (double and single precision arithmetic correspond to relative errors in the representation of any real number of approximately  $1.1 \times 10^{-16}$  and  $6.0 \times 10^{-8}$ ). AMHd and AMHs differ only in the choice of  $m$  and  $s$ , with AMHs being set up for single precision arithmetic and requiring fewer multiplications in all.

We compare the algorithms on four reaction networks, evaluating transitions of time  $t$  from an initial condition to a set of logarithmically-spaced  $t$  values up to a maximum of  $T = 40.27$ , which, in all examples, is a natural, large but reasonable value to consider. The first two examples lead to a  $1001 \times 1001$  rate matrix with a maximum (at  $t = T$ )  $\rho \approx 2014$  and  $2316$ ; the third leads to a  $5151 \times 5151$  rate matrix with a maximum  $\rho \approx 1573$  and the fourth to a  $12341 \times 12341$  matrix with a maximum  $\rho \approx 2416$ .

Our first example is the tractable immigration-death model (Example 5), where we used the same parameters as in Section 4.1, with  $n_{pop} = 1000$ . Our second example is the Moran model (Example 3) with  $n_{pop} = 1000$ ,  $X(0) = 50$  and  $\theta = (210.0, 20.0, 0.002, 0.0)$ . The parameter values imply that the state  $X = n_{pop}$  is absorbing and, more importantly, that the rate matrix is poorly conditioned and exponentiation is prone to producing large errors (see Crawford and Suchard, 2012). Finally,  $\mathbb{P}(X(T) \geq 980) \approx 0.960$ ; i.e., by the final time most of the population has the new allele. The third example is an SIR model (Example 1) for a population of  $n_{pop} = 100$  with  $(S(0), I(0)) = (99, 1)$ . Setting  $\theta = (1/n_{pop}, 0.25)$ , so that at the start of the epidemic an infective is expected to infect approximately four susceptibles, we find that  $\mathbb{P}(I(T) = 0) \approx 0.964$ ; there is a high probability that the epidemic is over by the final time considered. The final example is an SEIRS model with  $n_{pop} = 40$ ,  $(S(0), E(0), I(0)) = (39, 1, 0)$  and  $\theta = 1.5 \times (1/n_{pop}, 1.0, 0.25, 0.05)$  so that  $\mathbb{P}(E(T) + I(T) = 0) \approx 0.619$ , and epidemics that have not died out have typically suffered from two ‘waves’ of the disease.

In Figure 2 we first examine the immigration-death model, where accuracies are, effectively, exact. For values of  $\rho < 1$ , AMHs is much less accurate than AMHd, SPS2 and SPS2r, which all have similar accuracy. However, for larger values of  $\rho$ , AMHs, AMHd and SPS2 all have comparable accuracy, which degrades approximately linearly (on the log scale) as  $\rho$ , and hence the number of vector-matrix multiplications and, thus, the accumulated error, increases. The renormalisation step in SPS2r appears to mitigate against much of the degradation with  $\rho$ . Accuracy results for SPS with single-tailed truncation are indistinguishable from those for SPS with two-tailed truncation and so are not shown. For the four combinations of SPS with  $\epsilon = 10^{-9}$  (not shown), for  $\rho > 1$  accuracies are between  $10^{-10}$  and  $10^{-8.5}$ , with greater accuracy for  $\rho < 1$ . SPSr is the least accurate and SPS2 is the most accurate because arithmetic is still carried out to double precision so errors are entirely due to the premature truncation. SPS2 truncates with the upper tail at  $\epsilon/2$  and the lower strictly below  $\epsilon/2$  and so enjoys greater accuracy; the renormalisation in SPSr and SPS2r redistributes the missing mass over the existing entries rather than placing some of it on the entries which are currently zero yet should not be.

For small values of  $\rho$ ,  $\text{SPS}(\epsilon = 10^{-16})$  and AMHd have similar complexities, as do AMHs and  $\text{SPS}(\epsilon = 10^{-9})$ , this latter explaining the relative inaccuracy of AMHs compared with AMHd for low  $\rho$  values. For moderate and large  $\rho$  the complexities of  $\text{SPS}(\epsilon = 10^{-16})$  and  $\text{SPS}(\epsilon = 10^{-9})$  are very similar (since  $m \sim \rho$  for both) and are roughly half of an order of magnitude smaller than the complexities of both AMHd and AMHs. Indeed, at the largest



$\rho$  values the ratio for AMHd to SPS( $\epsilon = 10^{-16}$ ) is 0.249. The main reason for the efficiency gain is that to preserve precision in the face of potential cancellation of large positive and negative terms, the algorithm of Al-Mohy and Higham (2011) increases  $s$  so as to limit the highest series power to  $m = 55$ . For large  $\rho$  this leads to a cost of approximately  $5.6\rho$  and  $4.3\rho$  for AMHd and AMHs respectively, whereas for our algorithm, from Corollary 1, the cost is approximately  $\rho$ . The true cost of AMHs and AMHd, visible in Figure 2, is less than suggested above because, as described in Section 2.1, the algorithms include a stopping rule for early truncation of each series expansion.

Largely the same pattern as above is observed for the Moran, SIR and SEIRS models and so Figure 2 only includes the plots for the SIR model. The following minor differences are evident: (i) for low  $\rho$  values, AMHs is 5 (Moran), 3 (SIR) and 3 (SEIRS) rather than 6 orders of magnitude less accurate than AMHd and SPS( $\epsilon = 10^{-16}$ ); (ii) with no ground truth we are unable to ascertain the relative accuracies of AMHd and SPS( $\epsilon = 10^{-16}$ ) but can observe that their discrepancy increases with  $\rho$  and that they agree to within approximately  $10^{-15}$  for  $\rho \lesssim 100$ ; (iii) for SPS( $\epsilon = 10^{-9}$ ) renormalisation improves the accuracy slightly for the SIR and SEIRS models but reduces it slightly for the Moran and the Immigration-Death models. Using two-tailed truncation always improves the accuracy slightly. At the largest  $\rho$  values the ratio of complexities for AMHd to SPS( $\epsilon = 10^{-16}$ ) are 0.256 (Moran), 0.287 (SIR) and 0.332 (SEIRS).

For the algorithm of Al-Mohy and Higham (2011), because of the further complication of including the norm-approximation algorithm of Al-Mohy and Higham (2009), we did not approximate the norms  $\|\mathbf{M}^p\|$ , but calculated them exactly. The cost of these evaluations was not included in the algorithm complexity; the vector-matrix multiplications that would have been used for these calculations in Al-Mohy and Higham (2009) were also *not* included in the complexity.

### 4.3 Simultaneous evaluation at multiple time points

Finally, we investigate the MUSPS algorithm of Section 3.3; its accuracy, speed and usefulness. We examine the immigration-death and SEIRS algorithms with the parameterisation as specified in Section 4.2 and four variations on Barabasi-Albert random network model that will be described, briefly, below. For each system we considered  $n_t$  time points, equally spaced between 0 and  $t_{max}$ , where  $(n_t, t_{max}) = (2000, 50)$  for the immigration-death system,  $t_{max} = (200, 100)$  for the SEIRS system, and  $t_{max} = (200, 600)$  for each of the four the random networks; in each case the upper bound,  $t_{max}$ , was sensible given the system and (for SEIRS and random graphs) application of interest. Using 2000 time points for the intractable systems was not feasible as the cost of obtaining a set of approximate truths using SPS (see below) is quadratic in  $n_t$ .

We created a set of four random networks based upon a pair of independent realisations from the Barabasi-Albert model (see Appendix E),  $\mathcal{G}_A$  and  $\mathcal{G}_B$ , with parameters  $(n, m)$ . Each of  $\mathcal{G}_A$  and  $\mathcal{G}_B$  has  $n$  nodes, with an average degree of  $2m$ , a minimum degree of  $m$  and the probability that the degree of a randomly chosen node is  $k$  being proportional to  $k^{-3}$  (e.g. Durrett, 2007, Chapter 4). Our four graphs are obtained by connecting  $\mathcal{G}_A$  and  $\mathcal{G}_B$  through a single edge with a weight of  $m$ , as follows. Let  $h_A$  and  $h_B$  be the nodes in

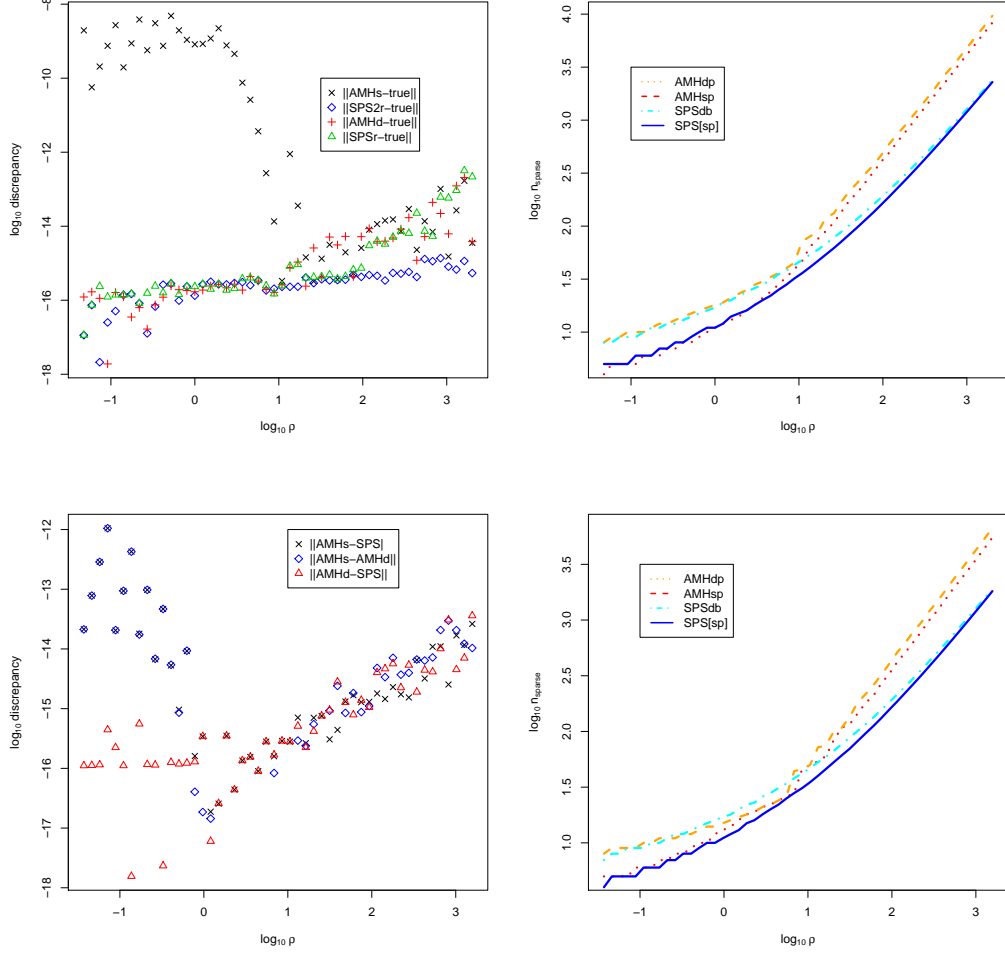


Figure 2: Accuracy and computational complexity for the immigration-death model (top) and the SIR network (bottom) when evaluating  $\nu_t^\top = \nu^\top e^{Qt}$ . In all panels the x-axis is  $\log_{10} \rho = \log_{10} t + \log_{10} \max_{i=1,\dots,d} |Q_{ii}|$ . The y-axis of the top-left panel shows the accuracy of each of AMHs, AMHd, SPS2r( $\epsilon = 10^{-16}$ ) and SPS( $\epsilon = 10^{-16}$ ), the bottom left panel shows the three possible discrepancies, between vectors evaluated using AMHs, AMHd and SPS2r( $\epsilon = 10^{-16}$ ); in each right panel the y-axis is  $\log_{10} n_{\text{sparse}}$  (excluding multiplications required for estimating  $\|Q^p\|^{1/p}$  for  $p = 2, \dots, 9$  in the methods of Al-Mohy and Higham (2011)) for AMHs, AMHd, SPS( $\epsilon = 10^{-9}$ ) and SPS( $\epsilon = 10^{-16}$ ).

Table 3: Timings for MUSPS and sequential SPS for: the immigration-death and SEIRS systems (5 repeats) and five realisations of  $\mathcal{G}_1$  as described in Section 4.3.

System	Imm-Death	SEIRS	Barabási-Albert ( $\mathcal{G}_1$ )
$d$	1000	12341	2000
$\rho t_{max}$	2500	6000	141600–232200
MUSPS (secs)	0.552–0.553	2.61–2.62	11.28–18.19
MUSPS/SPS	2.69–2.82	0.828–0.834	0.812–0.842

$\mathcal{G}_A$  and  $\mathcal{G}_B$  with the highest degree, and let  $\ell_A$  and  $\ell_B$  be the last node added to  $\mathcal{G}_A$  and  $\mathcal{G}_B$  respectively (this has the lowest possible degree). Joining  $h_A$  to  $h_B$  gives  $\mathcal{G}_1$ , joining  $h_A$  to  $\ell_B$  gives  $\mathcal{G}_2$ , joining  $\ell_A$  to  $h_B$  gives  $\mathcal{G}_3$  and joining  $\ell_A$  to  $\ell_B$  gives  $\mathcal{G}_4$ . We took  $n = 1000$  and  $m = 6$ .

For all three applications we ran MUSPS and a sequential SPS which evolved a current vector by a time of  $t_1 = t_{max}/n_t$  to obtain a new current vector  $n_t$  times. We compared the speeds of the two algorithms and their accuracies across all of the times from  $t_1$  to  $t_{max}$ ; for the immigration-death system, accuracy was relative to the known true transition probabilities; for the other two systems it was relative to an individual, direct calculation for each  $t$  using SPS. We used MUSPS2r and SPS2r throughout.

Each application was run 5 times; Table 3 shows the dimension and  $\rho t_{max}$  value for each system as well as the range of (i) times for MUSPS and (ii) ratios of the time for MUSPS to the time for sequential SPS. For the random networks model, for a given realisation of  $\mathcal{G}_A$  and  $\mathcal{G}_B$ , the variation in timings for  $\mathcal{G}_1, \dots, \mathcal{G}_4$  was less than 3%, so we only show the results for  $\mathcal{G}_1$ . Total time is roughly proportional to  $d\rho t_{max}$ , as expected. For SEIRS and the Barabási-Albert model MUSPS is more efficient than SPS. For the immigration-death system MUSPS is more expensive than sequential SPS for two reasons. Firstly, the dimension is small so the relative cost of the  $t$ -dependent overheads of the MUSPS algorithm is large; moreover,  $\mathbf{Q}$  has only 3 entries per column and so each vector-matrix multiplication has a similar cost to the vector-scalar multiplication and vector-vector addition that MUSPS must still perform. The additional cost may, however, be justified if accuracy is important, as we shall see.

Figure 3 plots the accuracy (base 10 logarithm of the  $L_1$  discrepancy from the ‘truth’, with  $t_1$  removed as all algorithms produce the same probability vector) of MUSPS against that of SPS for the immigration-death system, the SEIRS system and the first set of realisations from the random-network model (the pattern was persistent across replications). Whenever there is a substantial difference in the accuracies, MUSPS is more accurate than sequential SPS.

The left and central panels of Figure 4 demonstrates an example use of MUSPS within an SEIRS model by plotting the probability of extinction against  $t$  (left panel) and the expected number of people infected or exposed against  $t$  amongst infections which have not died out (central panel). The kink in the first graph around  $t = 15$  corresponds to the peak in the second. However, the central panel shows a dip in the presence of infections before (conditional) equilibrium is reached. Interestingly, the solution to the initial value

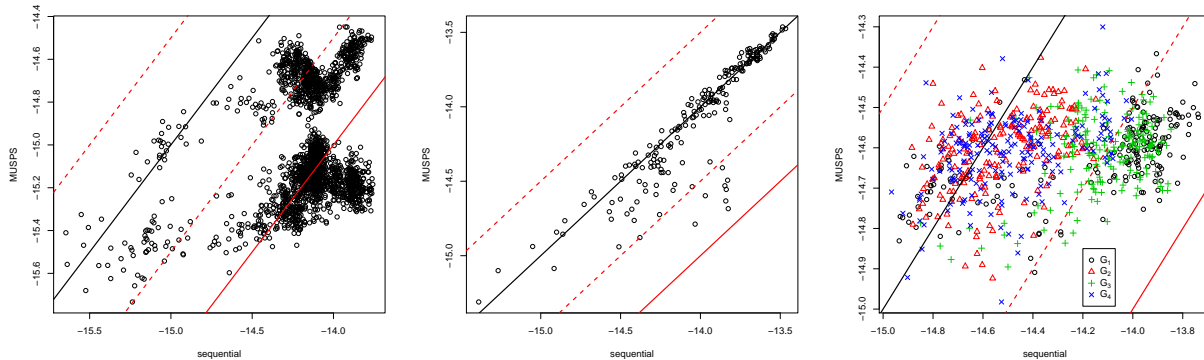


Figure 3: Accuracy ( $\log_{10}$ ) of estimates by MUSPS2r against accuracy of sequential SPS2r for  $n_t$  equally-spaced time points. Left panel: immigration-death; central panel: SEIRS; right panel Barabási-Albert. The line of equality is in black; the solid (dashed) red lines represent a discrepancy of one (one half of an) order of magnitude. For the central and right panels accuracy is estimated by approximating the truth using  $n_t = 200$  separate calculations via SPS2r.

problem with  $(S(0), E(0), I(0)) = (39, 1, 0)$  and

$$\frac{dS}{dt} = -\theta_1 SI + \theta_4(n_{pop} - S - E - I), \quad \frac{dE}{dt} = \theta_1 SI - \theta_2 E, \quad \frac{dI}{dt} = \theta_2 E - \theta_3 I, \quad (11)$$

mimics the conditional expectation well, but exaggerates the extrema.

The right panel of Figure 4 demonstrates the use of MUSPS to differentiate between different possible networks for the same set of vertices. A statistician may have several possible graphs for a network of known vertices for a variety of reasons: perhaps the network is incompletely or noisily observed or perhaps they wish to understand the sensitivity of information transmission to perturbations of the graph. In this, contrived, instance standard mechanisms for comparing  $\mathcal{G}_1, \dots, \mathcal{G}_4$ , such as the degree distribution or the maximal sub-graph (Burkea and Shearer, 1998), would suggest no difference between the graphs, yet the right-hand panel of Figure 4 show that the differences in information transmission are substantial. The graph shows  $d(\mathcal{G}_i, \mathcal{G}_j; t)$  as defined in (5) plotted against  $t$  when all the information is placed initially on the node of highest degree (e.g. the most influential member of the network releases some new information); the plot is for the first realisation of  $\mathcal{G}_A$  and  $\mathcal{G}_B$ , as the overall pattern was stable across realisations. It is clear directly from the plot, with no detailed examination of the graph structures that  $\mathcal{G}_2$  and  $\mathcal{G}_3$  are very similar, and are intermediate between  $\mathcal{G}_1$  and  $\mathcal{G}_4$  in terms of their information-transmission behaviour. In this instance the discrepancies will dwindle to zero since each  $\mathbf{Q}$  is symmetric, so  $e^{\mathbf{Q}t}$  is doubly stochastic and has a stationary distribution  $\propto 1$ .

## Acknowledgements

I would like to thank Prof. Lam Ho for suggesting that the reformulation of the statespace in Ho et al. (2018) in terms of births might be applicable within the methodology presented

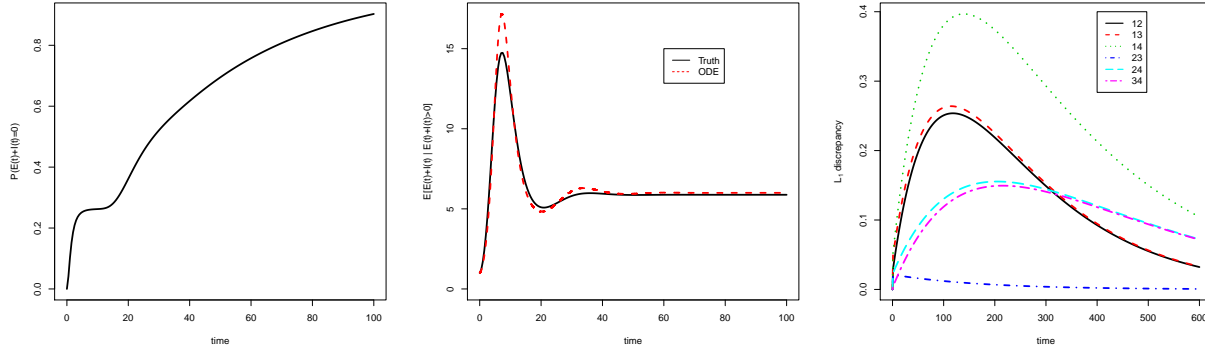


Figure 4: Left panel: probability that the SEIRS infection with parameters as specified in Section 4.2 has died out by time  $t$  against  $t$ ; centre panel:  $\mathbb{E}[E(t) + I(t) \mid E(t) + I(t) > 0]$  and the solution to the ODE in (11). Right panel:  $L_1$  discrepancies between transition probabilities against time for the four realisations of graphs described in the text.

herein. I am also grateful to Dr. Andrew Golightly for several useful discussions about reaction networks.

## References

- Al-Mohy, A. H. and Higham, N. J. (2009). A new scaling and squaring algorithm for the matrix exponential. *SIAM J. Matrix Anal. & Appl.*, 31(3):970–989.
- Al-Mohy, A. H. and Higham, N. J. (2011). Computing the action of a matrix exponential with an application to exponential integrators. *SIAM J. Sci. Comput.*, 33(2):488–511.
- Andersson, H. and Britton, T. (2000). *Stochastic Epidemic Models and Their Statistical Analysis*. Springer, New York, 1st ed. edition.
- Barabási, A. and Albert, R. (1998). Emergence of scaling in random network. *Science*, 286:509–512.
- Boucheron, S., Lugosi, G., and Massart, P. (2013). *Concentration inequalities [electronic resource] : a nonasymptotic theory of independence*. Oxford University Press, Oxford, 1st ed. edition.
- Burkea, H. and Shearer, K. (1998). A graph distance metric based on the maximal common subgraph. *Pattern Recognition Letters*, 19:255–259.
- Crawford, F. W. and Suchard, M. A. (2012). Transition probabilities for general birth-death processes with applications in ecology, genetics, and evolution. *Journal of Mathematical Biology*, 65(3):553–580.
- Durrett, R. (2007). *Random Graph Dynamics*. Cambridge University Press, Cambridge, 1st ed. edition.

- Gallopoulos, E. and Saad, Y. (1992). Efficient solution of parabolic equations by krylov approximation methods. *J. Applied Stat.*, 13(5):1236–1264.
- Georgoulas, A., Hillston, J., and Sanguinetti, G. (2017). Unbiased bayesian inference for population markov jump processes via random truncations. *Statistics and Computing*, 27(4):991–1002.
- Glynn, P. W. and Rhee, C.-H. (2014). Exact estimation for markov chain equilibrium expectations. *J. Appl. Probab.*, 51A:377–389.
- Hammond, D. K., Gur, Y., and Johnson, C. R. (2013). Graph diffusion distance: A difference measure for weighted graphs based on the graph laplacian exponential kernel. In *2013 IEEE Global Conference on Signal and Information Processing*, pages 419–422.
- Ho, L. S. T., Crawford, F. W., and Suchard, M. A. (2018). Direct likelihood-based inference for discretely observed stochastic compartmental models of infectious disease. *Ann. Appl. Stat.*, 12(3):1993–2021.
- Moler, C. and Van Loan, C. (2003). Nineteen dubious ways to compute the exponential of a matrix, twenty-five years later. *SIAM Review*, 45(1):3–49.
- R Core Team (2018). *R: A Language and Environment for Statistical Computing*. R Foundation for Statistical Computing, Vienna, Austria.
- Raggett, G. (1982). A stochastic model of the Eyam plague. *J. Applied Stat.*, 9(2):212–225.
- Saad, Y. (1992). Analysis of some krylov subspace approximations to the matrix exponential operator. *J. Applied Stat.*, 29(1):209–228.
- Sanderson, C. and Curtin, R. (2016). Armadillo: a template-based C++ library for linear algebra. *J. Open Source Software*, 1:26.
- Sanderson, C. and Curtin, R. (2018). A user-friendly hybrid sparse matrix class in C++. *LNCS*, 10931:422–430.
- Short, M. (2013). Improved inequalities for the Poisson and binomial distribution and upper tail quantile functions. *ISRN Probability and Statistics*, 2013(3):1–6.
- Sidje, R. B. (1998). EXPOKIT: a software package for computing matrix exponentials. *ACM Trans. Math. Soft.*, 24(1):130–156.
- Wilkinson, D. J. (2012). *Stochastic Modelling for Systems Biology*. CRC Press, Boca Raton, FL, 2nd ed. edition.

## A Proof of Theorem 1

The simple bounds arise because (i)  $r_0(\rho) = 1 - e^{-\rho} \leq \epsilon \Rightarrow m_\epsilon(\rho) = 0$ ; and (ii)  $r_1(\rho) = 1 - e^{-\rho}(1 + \rho) < \rho^2$  and since  $e^{-\rho} > 1 - \rho$ ,  $\rho \leq \sqrt{\epsilon} \Rightarrow r_1(\rho) \leq \epsilon$ , so  $m_\epsilon(\rho) \leq 1$ .

The other bounds all use aspects of the following result.

**Lemma 1.** Let  $h(x) := 1 - x + x \log x$ , then for  $x \geq 1$ ,

$$\frac{3}{6 + 2(x - 1)}(x - 1)^2 \leq h(x) \leq \frac{1}{2}(x - 1)^2.$$

*Proof.* The left hand inequality holds for  $x \geq 0$  and is from Boucheron et al. (2013) page 36. For the right hand inequality, set  $g(x) = (x - 1)^2/2$  and notice that  $0 = h(1) = g(1) = h'(1) = g'(1)$ , and  $h''(x) = 1/x \leq 1 = g''(x)$  for  $x \geq 1$ .  $\square$

The bound  $m_+$  arises from a standard Chernoff argument (e.g. Boucheron et al., 2013) for the right tail of a  $\text{Poisson}(\rho)$  random variable,  $X$ . The moment generating function is  $M_X(t) = \mathbb{E}[e^{Xt}] = \exp[\rho(e^t - 1)]$ , and by Markov's inequality:

$$\mathbb{P}(X \geq m) = \mathbb{P}(e^{Xt} \geq e^{mt}) \leq e^{-mt} M_X(t) = e^{-mt + \rho(e^t - 1)}.$$

The inequality holds for all  $t$  and the right-hand side is minimised at  $t = \log(m/\rho)$ , giving

$$\mathbb{P}(X \geq m) \leq \exp[-\rho h(m/\rho)] \leq \exp\left[-\rho \frac{3(m/\rho - 1)^2}{6 + 2(m/\rho - 1)}\right]$$

by Lemma 1. Setting  $\epsilon = \mathbb{P}(X \geq m + 1)$  and  $y = (m + 1)/\rho - 1$  gives  $3\rho y^2(6 + 2y) \log \epsilon \geq 0$ , from which  $y \geq -\log \epsilon \times \sqrt{1 - 18\rho/\log \epsilon}/(3\rho)$ , and (7) follows on substituting for  $y$ .

The much tighter bounds in (8) and (9) use Theorem 2 of Short (2013), which can be rewritten to state that

$$\Phi\left(-\sqrt{2\rho h(m'/\rho)}\right) < \mathbb{P}(X > m) < \Phi\left(-\sqrt{2\rho h(m/\rho)}\right), \quad (12)$$

where  $m' := m + 1$  and where the left hand side holds provided  $m' > \rho$  and the right hand side holds provided  $m > \rho$ . We first show that these conditions are satisfied. Firstly, when  $\rho < 1$ , clearly  $m' > \rho$ , moreover  $r_0(\rho) = 1 - e^{-\rho}$ , so provided  $1 - e^{-\rho} > \epsilon$ , we have  $m \geq 1 > \rho$ . When  $\rho \geq 1$ , we use the easily verified facts that  $r_m(m)$  is an increasing function of  $m$  and  $r_m(\rho)$  is an increasing function of  $\rho$ ; thus for  $\rho \geq m \geq 1$ ,  $r_m(\rho) \geq r_m(m) \geq r_1(1) = 1 - 2e^{-1} > 0.04$ , and the tolerance condition is not satisfied. We, therefore need  $m > \rho$ , which implies  $m' > \rho$ .

Neither  $\Phi^{-1}$  nor  $h^{-1}$  is tractable (functions that perform  $\Phi^{-1}(p)$  solve  $\Phi(x) = p$  iteratively), and even with the bounds on  $h$  from Lemma 1 and standard bounds on  $\Phi$  in terms of  $\phi$ , tractable inversion is still not possible. We use the bound (7) to create (8), and then (8) to create (9).

To prove (8), since  $\epsilon \leq 0.04$ , from the left inequality in (12),

$$0.04 \geq \mathbb{P}(X \geq m) \Rightarrow \sqrt{2\rho h(m'/\rho)} \geq -\Phi^{-1}(\epsilon) \approx 1.75 > \sqrt{3}.$$

Firstly, since  $m_+ + 1 \geq m + 1$ , this ensures  $A > 1$ , so  $\log(A - 1)$  is real. More importantly, it ensures that  $[2\rho h(m'/\rho)]^{-1/2} - [2\rho h(m'/\rho)]^{-3/2}$  is a decreasing function of  $[2\rho h(m'/\rho)]^{1/2}$  and, since  $h'(x) > 0$  for  $x > 1$ , it is also a decreasing function of  $m'$ . The  $m'$  that we desire satisfies  $m' \leq m_+ + 1 =: m'_+$ , and hence

$$[2\rho h(m'/\rho)]^{-1/2} - [2\rho h(m'/\rho)]^{-3/2} \geq [2\rho h(m'_+/\rho)]^{-1/2} - [2\rho h(m'_+/\rho)]^{-3/2}.$$

Since, for  $y > 0$ ,  $\Phi(-y) > (1/y - 1/y^3)\phi(y)$ ,

$$\Phi\left(-\sqrt{2\rho h(m'_+/\rho)}\right) \geq \{[2\rho h(m'_+/\rho)]^{-1/2} - [2\rho h(m'_+/\rho)]^{-3/2}\} \phi\left(\sqrt{2\rho h(m'_+/\rho)}\right).$$

Combining the left inequality in (12) with the right-hand inequality in Lemma 1 gives

$$\epsilon \geq \frac{1}{\sqrt{2\pi}} \{[2\rho h(m'_+/\rho)]^{-1/2} - [2\rho h(m'_+/\rho)]^{-3/2}\} \exp\left[-\frac{(m' - \rho)^2}{2\rho}\right].$$

Equation (8) follows on rearrangement.

To show (9) we apply the right hand inequality in (12) and the bound  $\Phi(-x) < \phi(x)/x$ , then the fact that  $m \geq m_-$ , and finally Lemma 1 to find:

$$\begin{aligned} \mathbb{P}(X > m) &< \frac{1}{\{4\pi\rho h(m/\rho)\}^{1/2}} \exp[-\rho h(m/\rho)] \leq \frac{1}{\{4\pi\rho h(m_-/\rho)\}^{1/2}} \exp[-\rho h(m/\rho)] \\ &\leq \frac{1}{\{4\pi\rho h(m_-/\rho)\}^{1/2}} \exp\left[-3\rho \frac{(x-1)^2}{6+2(x-1)}\right], \end{aligned}$$

where  $x = m/\rho$ . We must, therefore, ensure that the final bound is no more than  $\epsilon$ . Rearranging this gives  $3\rho(x-1)^2 - 2(B - \log \epsilon)(x-1) - 6(B - \log \epsilon) \leq 0$ , so that when  $B - \log \epsilon > 0$ ,  $x-1 \leq (B - \log \epsilon)(1 + \sqrt{1 + 18\rho/(B - \epsilon)})/(3\rho)$ .

## B Proof of Proposition 1

For any integer  $b$ , and  $1 \leq i \leq b$ ,

$$\frac{p_{b-i}}{p_{b+i}} = \rho^{-2i} b(b+1)(b-1)(b+2) \dots (b-i+1)(b+i) = \rho^{-2i} \left[b_*^2 - \frac{1}{2^2}\right] \dots \left[b_*^2 - \frac{(2i-1)^2}{2^2}\right]$$

where  $b_* = b + 1/2$ . Hence, if  $b_* \leq \rho$ ,  $p_{b-1}/p_{b+i} < 1$ , and so

$$\sum_{j=0}^{\lfloor b_* \rfloor - a - 1} p_i = \sum_{i=a+1}^{\lfloor b_* \rfloor} p_{b-i} < \sum_{i=a+1}^{\lfloor b_* \rfloor} p_{b+i} < \sum_{i=a+1}^{\infty} p_{b+i}.$$

## C MUSPS numerical underflow/overflow

The following lines should be added to Algorithm 3.3 to deal with possible numerical underflow or overflow for MUSPS2r.

## D Transition probabilities for Example 5

The model can be recast as  $n$  available slots, each of which is initially filled with a member of the species ( $X(0) = n$ ), and each of which evolves independently as a two-state Markov



---

**Algorithm 3** Additional lines for MUSPS algorithm for  $\nu^\top e^{\mathbf{Q}t_i}$  with  $t_1 < \dots < t_n$  and missing mass  $\leq \epsilon$ .

---

```

1:  $BIG \leftarrow 10^{100}$ ;  $SMALL \leftarrow 10^{-100}$ . ▷ insert after line 1
2: if  $b > BIG$  then ▷ insert after line 4
3:    $\nu \leftarrow \nu/b$ ;  $b \leftarrow 1$ .
4: if  $b > BIG$  or  $g_{i_{lo}} < SMALL$  then ▷ insert after line 17
5:    $\nu_{sum,i} \leftarrow \nu_{sum,i}/(b * g_i)$  ( $i = i_{lo}, \dots, i_{hi}$ ).
6:    $g_i \leftarrow 1$  ( $i = i_{lo}, \dots, i_{hi}$ ).
7:    $\nu_{pro} \leftarrow \nu_{pro}/b$ ;  $b \leftarrow 1$ .

```

---

chain that switches from full to empty with rate a rate of  $\mu$  and from empty to full with a rate of  $\gamma$ . The probability that a given slot is full at time  $t$  is  $p(t) = (\gamma + \mu e^{-(\gamma+\mu)t})/(\gamma + \mu)$ , and hence the  $i$ th ( $i = 0, \dots, n$ ) entry of  $\nu(t)$  is

$$\mathbb{P}(X(t) = i) = \frac{N!}{i!(N-i)!} p(t)^i [1 - p(t)]^{N-i},$$

which is calculated using `long double` precision.

## E The Barabási-Albert Model

There are several possible versions of the model defined in Barabási and Albert (1998); we use the precise version defined in (Durrett, 2007, Chapter 4). The model has two integer parameters,  $n$  and  $m$ , and starts with 2 nodes and  $2m$  edges connecting the two. New nodes are added sequentially until there are  $n$  nodes. When it is added, a new node has  $m$  edges emanating from it. These too are added sequentially, with the node at the other end of the edge chosen from all existing nodes (except the one being added) with a probability proportional to its degree. Once all nodes have been added, where any pair of nodes is connected by  $k > 1$  edges, these edges are combined into a single edge with a weight of  $k$ .